Emergence, Induction, and Control of Re-Entrant Dynamics in an Excitable Cellular Automaton

Katherine Langille[1]

[1]Department of Systems Design Engineering, University of Waterloo, Canada
klangill@uwaterloo.ca

Abstract

Excitable media cellular automata provide a minimal framework for studying the emergence and control of complex spatiotemporal dynamics. This work presents a systematic investigation of rhythm breakdown and recovery in a two-dimensional Greenberg–Hastings cellular automaton modelling excitable tissue. Across three experimental phases, we examine how substrate properties, external perturbations, and structural interventions govern the onset and persistence of re-entrant activity. First, spontaneous re-entry arises only when a critically short refractory period coincides with structural heterogeneity, indicating a sharp transition in system dynamics. Second, a premature cross-field stimulation protocol maps the parameter regimes in which re-entry can be induced, showing that the vulnerable window expands as the refractory period decreases and becomes effectively unbounded in a critical regime. Third, inexcitable obstacles are used to test structural control, showing that termination depends on occluding the re-entrant source, while incomplete or misaligned barriers allow persistent dynamics through circumnavigation. The observed re-entrant patterns differ from classical spiral waves, instead behaving as periodic source-like emitters due to discrete recovery dynamics and local excitation thresholds. These results show how complex self-sustaining behaviours emerge from simple local rules and how their controllability depends on structural and dynamical constraints. More broadly, this work highlights how minimal excitable systems can serve as tractable models for studying emergence, phase transitions, and control in artificial life.

Data/Code available at: `https://github.com/Bananagoo/alife2026-excitable-ca-reentry`

Introduction

Excitable media are systems composed of local units that can be activated, recover, and later become activatable again. Examples include chemical reactions, neural tissue, cardiac tissue, and cellular automata. These systems are central to artificial life because complex global patterns can emerge from simple local rules without a centralized controller. In this paper, I study one such system using a Greenberg–Hastings cellular automaton (GH-CA): a rule-based excitable-medium model in which each cell cycles through resting, excited, and refractory states, and excitation spreads through neighbouring cells (Greenberg and Hastings, 1978; Weimar et al., 1992).

The motivating biological case is atrial fibrillation (AF), a sustained cardiac arrhythmia associated with impaired cardiac contraction and turbulent blood flow (Pandit and Jalife, 2013). In excitable-media terms, AF can be understood as a breakdown of coherent wave propagation. Instead of one ordered activation wave passing through tissue and extinguishing, excitation may become trapped in a self-sustaining loop. This process is called re-entry: a wave repeatedly reactivates tissue that has recovered enough to be excited again. Re-entry is often associated with spiral waves or rotors, which can act as persistent sources of abnormal activation (Pertsov et al., 1993; Pandit and Jalife, 2013).

This work uses the cardiac setting as an application domain, but the broader question is an artificial-life one: under what conditions can simple local excitation rules produce persistent global activity, and when can that activity be controlled? Previous work has shown that minimal cellular automata can generate planar waves, spiral waves, and disordered regimes (Greenberg and Hastings, 1978; Weimar et al., 1992; Reyes and Laroze, 2022). This paper contributes a systematic three-part study within one minimal framework: spontaneous onset, induced onset, and structural termination of re-entrant dynamics. The goal is not to produce a clinically detailed cardiac model, but to use an abstract excitable medium to identify how parameter regimes, perturbation timing, and obstacle geometry shape emergent behaviour.

Three experimental phases are reported. Phase 1 varies refractory period and structural heterogeneity to determine when re-entry occurs without an external trigger. Phase 2 applies a premature cross-field stimulus, corresponding to the standard cardiac S1–S2 protocol, to map the timing window in which re-entry can be induced. Phase 3 introduces per-

manently inexcitable regions, analogous to ablation lesions or obstacles, to test which geometries terminate sustained activity. Together, these phases test three hypotheses. *H1:* shortening the refractory period makes re-entry possible, but does not destabilize a homogeneous planar wave without a second factor such as structural heterogeneity or an external perturbation. *H2:* premature stimulation induces re-entry only inside a vulnerable timing window. *H3:* termination depends on lesion geometry and placement relative to the re-entrant source.

The results show a sharp transition in system behaviour. Spontaneous re-entry occurs only when a critically short refractory period coincides with fibrotic heterogeneity. Premature stimulation expands the inducible regime, with the vulnerable window widening as the refractory period decreases. Structural intervention succeeds only when it occludes the source of re-entry. These findings emphasize that emergent excitable-media dynamics are controllable only when intervention geometry respects the topology and timing of the underlying wave process.

Background and Related Work

Cardiac tissue is an excitable medium in which electrical waves propagate to coordinate contraction. Under normal conditions, excitation initiated by the sinoatrial node, the heart's natural pacemaker region, spreads coherently and extinguishes when it reaches refractory tissue or anatomical boundaries. Pathological conditions can destabilize this propagation, allowing wavefronts to fragment into spiral waves or rotors (Pertsov et al., 1993; Pandit and Jalife, 2013). In continuous models, a rotor typically consists of a curved wavefront rotating around a phase singularity where excitation and recovery meet.

Biophysically detailed cardiac models usually describe transmembrane voltage and ionic currents with systems of ordinary or partial differential equations. Many such models are also solved on spatial grids using finite-difference or related numerical methods, so the distinction between cellular automata and detailed electrophysiology is not simply grid-based versus non-grid-based modelling. The practical difference is that detailed reaction–diffusion models compute richer per-cell electrophysiological updates, while cellular automata use a small discrete state set and local transition rules (Romitti et al., 2025; Song, 2023). This abstraction reduces physiological realism but makes broad parameter sweeps and mechanism-focused experiments more tractable.

The Greenberg–Hastings model showed that a minimal excitable cellular automaton can generate complex spatial patterns through local diffusion rules alone (Greenberg and Hastings, 1978). Later work on cellular automata and excitable networks demonstrated that refractory timing, spatial coupling, and network disorder can shift systems between ordered travelling waves, rotating waves, and turbulent regimes (Bhattacharya and Iglesias, 2019; Reyes and Laroze, 2022). In cardiac modelling, refractory period shortening reduces excitation wavelength, allowing re-entrant circuits to fit into smaller spatial regions (Pandit and Jalife, 2013). Structural heterogeneity such as fibrosis can create conduction block, wavebreak, and anchoring sites for re-entry (de Groot and Nattel, 2015; Alonso et al., 2016).

A common way to initiate re-entry experimentally and computationally is the S1–S2 cross-field protocol. The S1 wave is a conditioning wave that creates a spatial gradient of recovery. A later S2 stimulus is delivered perpendicular to this wave. If S2 arrives while part of the tissue is excitable and part is still refractory, one side of the induced wave can propagate while the other is blocked. This asymmetry produces a free wave tip that may curl into re-entry (Pertsov et al., 1993; Winfree, 1989). The timing interval in which this occurs is called the vulnerable window.

Structural interventions such as catheter ablation work by making selected regions electrically inactive or disconnected (Cheniti et al., 2018). Computational work shows that spiral waves interact strongly with inexcitable obstacles and may be pinned, redirected, or terminated depending on lesion geometry and placement (Kuklik et al., 2013; Trayanova, 2014). This makes ablation a useful analogue for studying control of emergent dynamics in excitable media: adding structure can suppress global activity, but can also leave pathways for continued circulation if the geometry is incomplete.

Methods

Model Architecture

The simulation uses a two-dimensional square grid of size $L \times L$, with $L = 180$. Each cell $C_{i,j}$ occupies an integer state in the range $0, \ldots, N$, where N determines the length of the refractory recovery cycle. State 0 is resting and excitable, state 1 is excited, states 2 through $s_{\mathrm{rrp}} - 1$ are absolutely refractory, states s_{rrp} through $N-1$ are relatively refractory, and state N is the final recovery state before returning to rest. The quantity s_{rrp} is the state at which the relative refractory period begins, defined below.

A separate tissue mask encodes normal, fibrotic, and ablated cells. Normal conducting cells have `fiber` value 0, fibrotic cells have `fiber` value 1, and ablated cells have `fiber` value 2. Fibrotic and ablated cells are permanently inexcitable, remain fixed in the resting state, and do not transmit excitation. The grid updates synchronously at each timestep over the Moore neighbourhood, meaning each cell is coupled to its eight nearest neighbours.

Fibrosis Generation

Structural heterogeneity is represented as a spatially correlated inexcitable mask. The purpose of this mask is not to reproduce patient-specific fibrosis, but to create patchy and strand-like conduction obstacles resembling idealized interstitial fibrosis. The mask combines three components:

a smooth background density field generated by randomly placed Gaussian kernels, curved strand-like features generated by random walks, and irregular ellipsoidal patches representing focal obstacles. These components are combined into a probability map, and cells are sampled until the target fibrosis fraction is reached (Alonso et al., 2016). Column 0, which represents the pacemaker column, is excluded from fibrosis placement so that pacing remains possible.

Update Rules and Relative Refractoriness

The standard GH excitation rule is augmented with a relative refractory period (RRP), representing graded recovery of excitability (Kl'eber and Rudy, 2004). The refractory interval is divided into absolute and relative portions. The first relative refractory state is

$$s_{\mathrm{rrp}} = \lfloor N(1-\alpha_{\mathrm{rrp}}) \rfloor, \tag{1}$$

where $\alpha_{\mathrm{rrp}} \in [0,1]$ is the fraction of the refractory interval treated as relatively refractory. Across all experiments, $\alpha_{\mathrm{rrp}} = 0.5$.

The update rules are as follows. A resting cell becomes excited if at least one Moore neighbour is excited. An excited cell advances to state 2 on the next timestep. A cell in the absolute refractory range increments by one each timestep and cannot be re-excited. A relatively refractory cell can be re-excited only if enough neighbours are excited. The required number of excited neighbours is the state-dependent threshold

$$\theta(s) = \left\lceil \frac{8(N-s)}{N - s_{\mathrm{rrp}}} \right\rceil, \tag{2}$$

where s is the current state of the cell, 8 is the number of Moore neighbours, and s_{rrp} is the beginning of relative refractoriness. This threshold decreases from 8 at the start of the relative refractory period to 1 near full recovery. Cells in state N return to resting state 0 on the following timestep. Fibrotic and ablated cells remain fixed and do not update.

Pacing and Evaluation Metrics

Normal sinus rhythm is simulated by forcing all non-fibrotic cells in the leftmost column into the excited state. This column represents the sinoatrial-node pacing boundary. A new paced wave is initiated only after the previous paced wave has extinguished and at least $T_{\mathrm{pace}} = 22$ timesteps have elapsed.

The primary activity signal is the number of excited cells at time t:

$$A(t) = \sum_{i,j} \mathbf{1}\left[C_{i,j}(t) = 1\right]. \tag{3}$$

This definition is used both to detect sustained excitation and to compute summary metrics. The baseline paced activity $\langle A_{\mathrm{pace}} \rangle$ is measured for each N from a pacemaker-only simulation with no fibrosis and no external perturbation.

Three metrics quantify global behaviour. Excess activity is

$$\Delta A = \langle A(t) \rangle - \langle A_{\mathrm{pace}} \rangle, \tag{4}$$

where the average is taken over the relevant observation window. Activity variance is

$$\sigma_A^2 = \mathrm{Var}[A(t)], \tag{5}$$

which captures temporal irregularity. Spatial disorder is measured using Shannon entropy,

$$H = -\sum_k p_k \ln(p_k), \tag{6}$$

where p_k is the fraction of cells in macro-state $k \in \{\mathrm{resting}, \mathrm{excited}, \mathrm{refractory}\}$. These metrics are reported because sustained re-entry generally produces elevated activity, temporal fluctuation, and mixed spatial states compared with paced propagation.

Experimental Phases

Phase 1: Substrate Characterisation Phase 1 tests whether substrate properties alone can generate spontaneous re-entry. The refractory period and fibrosis percentage are swept across a 10×6 parameter grid. Tested values are

$$N \in \{2, 3, 4, 5, 6, 8, 10, 12, 16, 20\} \tag{7}$$

and fibrosis fractions of 0, 5, 10, 20, 30, and 40 percent. Each simulation begins from pacemaker-only conditions and runs for

$$5(T_{\mathrm{pace}} + L + N) \tag{8}$$

timesteps with pacing active and no external perturbation. Spontaneous re-entry is scored as present when $A(t)$ does not return to zero after a warm-up period beginning at

$$t = T_{\mathrm{pace}} + L + N. \tag{9}$$

The three metrics ΔA, σ_A^2, and H are computed over the same post-warm-up window.

Phase 2: Premature Cross-Field Stimulation Phase 2 tests induction by a premature stimulus. A conditioning S1 plane wave is driven from the left pacing column. A premature S2 stimulus is then applied as a short horizontal line of excited cells, perpendicular to the S1 wavefront. The stimulus is delivered at row $r = 90$, centred at column $c = 90$, with half-length 10 cells. The S2 delay is measured relative to the time at which the left edge of the S1 wavefront reaches the left edge of the S2 line. The S2 stimulus excites cells that are resting or relatively refractory, while leaving absolutely refractory cells unchanged, thereby creating the asymmetric excitability needed for wavebreak (Pertsov et al., 1993; Winfree, 1989).

The sweep covers $N \in \{2, 3, \ldots, 20\}$ and S2 delays from 0 to 42 timesteps, giving 817 tested combinations. After S2

delivery, the pacing column is disabled so that later pacing does not mask the induced dynamics. Re-entry is scored as present if excitation persists in the interval

$$t \in [t_{\mathrm{S2}} + L - 1,\ t_{\mathrm{S2}} + L + 2T_{\mathrm{pace}}], \tag{10}$$

where t_{S2} is the S2 delivery time.

Phase 3: Ablation Geometry Phase 3 tests structural control. A stable re-entrant state is first produced using $N = 4$ and S2 delay equal to 13 timesteps, with pacing disabled after S2. After 120 timesteps of post-S2 evolution, an ablation geometry is stamped onto the grid at

$$t = t_{\mathrm{S2}} + 120. \tag{11}$$

In the selected trial this corresponds to $t = 213$. The simulation then continues for 400 additional timesteps. Six conditions are evaluated: an unablated control; a circular spot lesion of radius 15 cells centred at the re-entrant source; a three-sided C-shaped barrier; a two-sided L-shaped barrier; a closed rectangular ring; and a filled rectangular block. Termination is defined as $A(t)$ reaching zero and remaining zero for at least $2T_{\mathrm{pace}} = 44$ consecutive timesteps after ablation.

Results

Phase 1: Substrate Characterisation

Across the 60 tested substrate combinations, spontaneous re-entry occurred only at $N = 3$ with fibrosis greater than or equal to 5 percent. All other conditions, including all homogeneous substrates and all $N = 2$ cases, produced only paced wavefronts that propagated and extinguished. This supports H1: refractory-period shortening alone did not destabilize coherent propagation; structural heterogeneity was also required.

The metrics at $N = 3$ show a sharp transition (Table 1). With no fibrosis, the system remains paced and ΔA is zero. At 5 percent fibrosis, ΔA increases to $+14{,}269$, σ_A^2 reaches 120,758, and H increases to 0.916 nats. Higher fibrosis levels continue to support re-entry but reduce ΔA, reflecting loss of excitable tissue to non-conductive obstacles.

Table 1: Phase 1 metrics at $N = 3$ across fibrosis levels.

Fibrosis	ΔA	σ_A^2	H	Re-entry
0 percent	0	157	0.095	No
5 percent	14269	120758	0.916	Yes
10 percent	12838	17272	1.009	Yes
20 percent	9964	2606	1.089	Yes
30 percent	7256	870	1.068	Yes
40 percent	5163	1820	0.982	Yes

Within this re-entrant island, ΔA decreases monotonically from 5 percent to 40 percent fibrosis. Activity variance falls strongly from 5 percent to 30 percent fibrosis and rises slightly at 40 percent, suggesting that higher obstacle density constrains the dominant activity while still allowing intermittent local fragmentation. Entropy remains near 1.0 nats across the re-entrant cases, consistent with persistent mixed-state spatial structure. Figure 2 contrasts the dense multi-wavelet activity at $N = 3$ with extinguishing propagation at $N = 16$ under the same high fibrosis level.

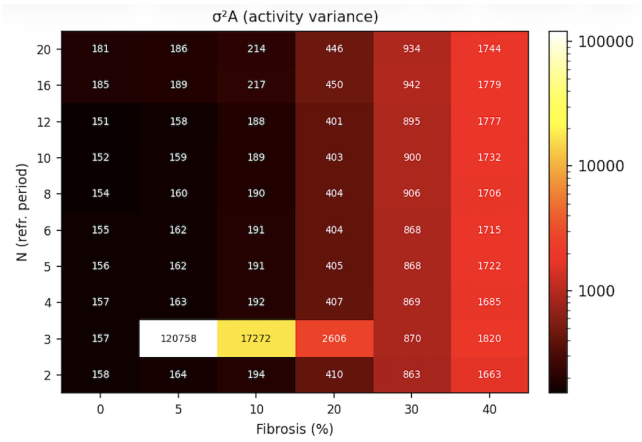

Figure 1: Phase 1 activity variance σ_A^2 across the $N \times$ fibrosis parameter sweep. Elevated variance is confined to $N = 3$ with fibrosis greater than or equal to 5 percent, matching the observed re-entry boundary.

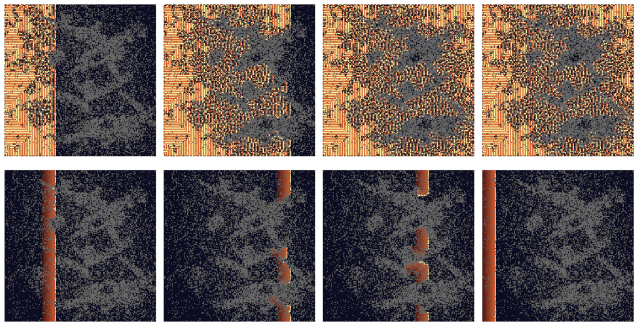

Figure 2: Phase 1 snapshots at $t \in \{60, 150, 320, 600\}$. Top: $N = 3$, fibrosis equal to 35 percent, where short refractory timing permits sustained fragmented activity. Bottom: $N = 16$, fibrosis equal to 35 percent, where wavefronts attenuate and extinguish. Colour scale: black = resting, yellow = excited, orange/dark red = refractory, grey = fibrosis.

Phase 2: Premature Cross-Field Stimulation

Premature stimulation induced re-entry for $N \leq 6$, but the timing regime depended strongly on refractory period. For $N \in \{2, 4, 5, 6\}$, re-entry occurred within bounded vulnerable windows: delays 1–22 for $N = 2$, 3–22 for $N = 4$, 4–22 for $N = 5$, and 5–22 for $N = 6$. At $N = 3$, re-entry

occurred for every S2 delay tested from 0 to 42 timesteps. No re-entry was induced for $N \geq 7$.

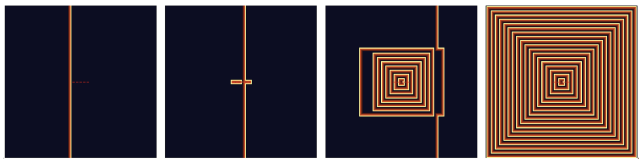

Figure 3: Phase 2 induction at $N = 4$, S2 delay equal to 13. From left: S1 plane wave before S2, state just after S2 delivery, rotor formation, and sustained square re-entry. The red dashed line indicates the S2 stimulus position.

Entropy confirms this induction boundary (Fig. 4). Within the vulnerable window, H reached approximately 0.95, 0.88, 0.85, and 0.75 nats for $N = 2, 3, 4$, and 6, respectively. Excess activity reached approximately $+8{,}500$ for $N = 2$, $+11{,}033$ for $N = 3$, $+5{,}100$ for $N = 4$, and $+3{,}600$ for $N = 6$. Activity variance peaked near 2.5×10^7 at $N = 3$, indicating chaotic multi-wavelet activity rather than the more periodic single-source dynamics observed for larger inducible N.

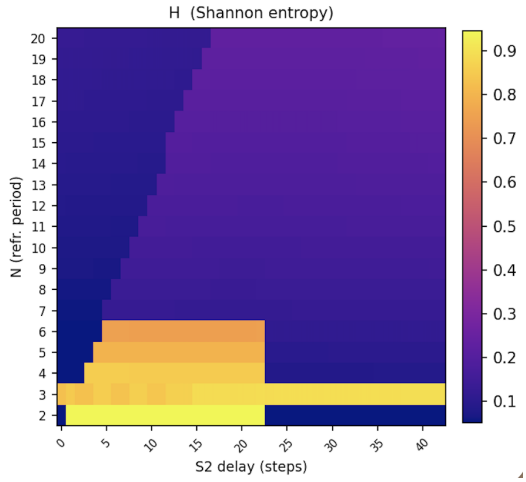

Figure 4: Phase 2 parameter sweep. Shannon entropy H in (N, δ_{S2}) space. Re-entry is bounded in timing for $N \in \{2, 4, 5, 6\}$, while $N = 3$ remains elevated across the full tested delay range.

Figure 5 shows the local induction mechanism. Cells excited by S2 complete the GH recovery cycle and become excitable near the centre of the broken wave. The free tips created at the ends of the S2-induced break curl along the refractory–excitable boundary and re-excite recovered cells. The resulting secondary wave expands outward with a gap where surrounding tissue remains refractory, producing new free tips. Repetition of this process produces sustained re-entry.

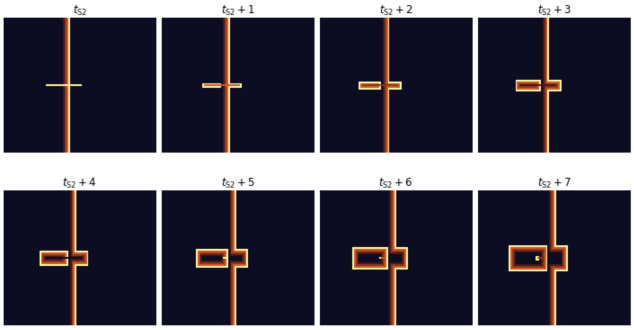

Figure 5: S1–S2 rotor induction detail for $N = 4$, S2 delay equal to 13. Each panel shows an 80×90 subregion centred on the stimulus site. Colour scale: dark blue = resting, yellow = excited, orange–dark red = early–late refractory.

Phase 3: Ablation Geometry

Two ablation geometries terminated re-entry and three did not (Table 2). The circular spot lesion and filled rectangular lesion both stopped sustained activity. In both cases, excitation persisted briefly after ablation and then collapsed to zero without recurrence.

Table 2: Phase 3 ablation outcomes.

Condition	Cells	Geometry	Terminated
Control	0	–	No
Spot ($r = 15$)	709	Circle	Yes
Box, 1 side open	133	C-shape	No
Box, 2 sides open	89	L-shape	No
Box, closed	176	Ring	No
Box, filled	2025	Solid	Yes

The C-shaped and L-shaped barriers failed because the wavefront could travel around the open boundary and re-establish activity in the remaining excitable space. The closed ring failed for a different reason: although it formed a complete obstacle, it did not occlude the re-entrant source. Activity persisted inside the ring, with the ring acting as a confining boundary rather than a terminating lesion. These results support H3, but more specifically indicate that source occlusion, not geometric completeness alone, determines termination in this model.

Discussion

Substrate Modification and Critical Behaviour

Phase 1 demonstrates that spontaneous re-entry depends on a narrow interaction between refractory timing and structure. Neither a short refractory period alone nor fibrosis alone was sufficient. The system entered a self-sustaining regime only at $N = 3$ with fibrotic obstacles present. This is consistent with the idea that electrical remodelling shortens excitation

wavelength, while structural heterogeneity supplies sites of conduction block and wavebreak (Nattel, 2002; de Groot and Nattel, 2015; Heijman et al., 2018).

The critical behaviour at $N = 3$ aligns with previous theoretical work showing that transitions between travelling waves, spirals, and failed propagation depend on ratios of refractory time scale to spatial coupling (Bhattacharya and Iglesias, 2019). In this model, $N = 3$ appears to sit near the boundary where wavebreaks introduced by fibrosis can curl into persistent re-entry. The failure of $N = 2$ to produce spontaneous re-entry suggests a lower bound: recovery is so rapid, and interaction with fibrotic barriers so abrupt, that no stable orbit is formed without an external trigger.

Increasing fibrosis within the re-entrant island reduces the amount of excitable tissue available to sustain activity. This explains the monotonic decline in ΔA and is consistent with critical-mass arguments for fibrillation maintenance (Qu et al., 2006). From an ALife perspective, this narrow regime resembles an edge-of-chaos transition: complex self-sustaining dynamics arise only in a constrained parameter region between orderly extinction and failed organization (Langton, 1996).

Induction by Premature Stimulation

Phase 2 shows that the vulnerable window expands as refractory period decreases. Shorter refractory periods reduce excitation wavelength and enlarge the excitable gap behind the conditioning wave. A premature S2 stimulus can exploit this partial recovery over a broader range of timings, producing wavebreak and re-entry. The approximately fixed upper boundary near delay 22 indicates a model-specific recovery point: once the S1 refractory tail has fully recovered, the S2 stimulus no longer encounters enough asymmetry to form a free tip.

The $N = 3$ case is qualitatively distinct. Re-entry occurred at all tested S2 delays, suggesting a critical regime in which the substrate is so close to self-sustaining dynamics that almost any perturbation can initiate persistent activity. This result should not be interpreted as a universal property of cardiac tissue; it is a property of the discrete GH-CA rules and selected pacing geometry. It is nevertheless useful because it identifies a phase-like transition in controllability and inducibility.

The induced patterns also differ from classical Archimedean spiral waves. Instead of a single rotating arm around a quiescent core, the model often produces a periodic source-like emitter. This occurs because the relative refractory threshold permits cells near state $N - 1$ to be re-excited by a small number of excited neighbours. The central region therefore refires periodically and emits outward wavefronts. The Moore neighbourhood further imposes a square lattice geometry, producing square or concentric wavefronts rather than smooth circular spirals. This distinction is important: the model captures re-entrant persistence, but the morphology is shaped by discrete recovery and lattice effects.

Ablation and Structural Control

Phase 3 indicates that successful termination requires occlusion of the re-entrant source. The spot and filled lesions both removed the cells responsible for maintaining the periodic source-like emitter. Once the source was eliminated, remaining waves propagated outward and died at boundaries or refractory tissue. This parallels the logic of pulmonary vein isolation in AF treatment, where ablation targets source regions or triggers rather than every propagating wavefront (Ha"issaguerre et al., 1998; Cheniti et al., 2018).

Incomplete barriers failed because they preserved a path for circumnavigation. The closed ring shows an additional constraint: a complete barrier can still fail if it surrounds rather than removes the source. This supports computational and clinical observations that gaps, incomplete lines, or misplaced lesions can allow re-entry to continue or reorganize (Spector and Bates, 2012; Lim et al., 2016; Trayanova, 2014). More generally, control of emergent excitable-media dynamics depends on topology. A barrier is effective only when it intersects the generative structure of the dynamics.

ALife Significance

This work is relevant to artificial life because it demonstrates how persistent, structured, and controllable global behaviour can emerge from a small set of local update rules. The cells contain no representation of a rotor, vulnerable window, or ablation target. These behaviours arise through interactions among local excitation, recovery timing, spatial coupling, and inexcitable structure.

The model also illustrates the value of minimal abstraction. Detailed reaction–diffusion models remain necessary for physiological prediction, but a cellular automaton makes it easier to map broad parameter regimes and isolate mechanisms. The distinction is not that detailed models cannot be simulated on grids, but that their per-cell updates encode substantially more biophysical state. The GH-CA sacrifices that detail to expose qualitative relationships among refractoriness, heterogeneity, perturbation timing, and structural control. For ALife, this is the core contribution: a clinically inspired excitable system becomes a tractable model for emergence, phase transitions, and intervention in complex adaptive media.

Limitations

Several limitations constrain interpretation. First, the GH-CA does not model action-potential morphology, calcium dynamics, anisotropic fibre orientation, or gap-junction remodelling, all of which influence cardiac wave stability (de Groot and Nattel, 2015; Heijman et al., 2018). Second, the model is two-dimensional and uses an idealized square lattice rather than realistic atrial anatomy. Third, fibrosis

generation is stochastic, but the reported Phase 1 sweep uses one generated morphology per fibrosis level. The sharp boundary should therefore be interpreted as the outcome for these sampled masks, not as an ensemble probability of re-entry. Future work should repeat each parameter combination over many independently generated fibrosis masks and report distributions of ΔA, σ_A^2, H, and re-entry frequency. Fourth, Phase 3 uses a single induced source state and a limited set of lesion geometries. A more complete study should vary lesion size, placement, and initial rotor morphology.

Conclusion

This paper presented a systematic study of re-entrant dynamics in a minimal two-dimensional Greenberg–Hastings cellular automaton. Spontaneous re-entry appeared only under a narrow combination of a critically short refractory period and structural heterogeneity. Premature cross-field stimulation expanded the re-entrant regime, with the vulnerable window widening as refractory period decreased and becoming effectively unbounded at the critical $N = 3$ condition. Structural intervention terminated sustained activity only when it occluded the re-entrant source; incomplete or misaligned barriers allowed continued activity through circumnavigation or confinement.

These results show how self-sustaining dynamics can arise from simple local excitation rules and how their control depends on both dynamical timing and structural geometry. Beyond the cardiac motivation, the model provides a compact artificial-life system for studying emergence, phase transitions, and controllability in excitable media.

Acknowledgements

This work was developed in the context of SYDE 537, taught by C. L. Nehaniv at the University of Waterloo.

References

Alonso, S., B"ar, M., and Echebarria, B. (2016). Nonlinear physics of electrical wave propagation in the heart: a highly spatiotemporal model. *Reports on Progress in Physics*, 79(9):096601.

Bhattacharya, S. and Iglesias, P. A. (2019). Controlling excitable wave behaviors through the tuning of three parameters. *Biological Cybernetics*, 113:61–70.

Cheniti, G., Vlachos, K., Pambrun, T., Hooks, D., Frontera, A., Takigawa, M., Bourier, F., Kitamura, T., Martin, C., Duchateau, J., et al. (2018). Atrial fibrillation mechanisms and implications for catheter ablation. *Frontiers in Physiology*, 9:1458.

de Groot, N. M. S. and Nattel, S. (2015). Cardiac fibrosis in patients with atrial fibrillation: mechanisms and clinical implications. *Journal of the American College of Cardiology*, 65(22):2388–2396.

Greenberg, J. M. and Hastings, S. P. (1978). Spatial patterns for discrete models of diffusion in excitable media. *SIAM Journal on Applied Mathematics*, 34(3):515–523.

Ha"issaguerre, M., Ja"is, P., Shah, D. C., Takahashi, A., Hocini, M., Quiniou, G., Garrigue, S., Le Mouroux, A., Le M'etayer, P., and Cl'ementy, J. (1998). Spontaneous initiation of atrial fibrillation by ectopic beats originating in the pulmonary veins. *New England Journal of Medicine*, 339(10):659–666.

Heijman, J., Algalarrondo, V., Voigt, N., Melka, J., Dobrev, D., Nattel, S., and Vigmond, E. J. (2018). The value of basic research insights into atrial fibrillation mechanisms as a guide to therapeutic innovation: a critical analysis. *Frontiers in Physiology*, 9:1221.

Kl'eber, A. G. and Rudy, Y. (2004). Basic mechanisms of cardiac impulse propagation and associated arrhythmias. *Physiological Reviews*, 84(2):431–488.

Kuklik, P., Sanders, P., Szumowski, L., and Zebrowski, J. J. (2013). Attraction and repulsion of spiral waves by inhomogeneity of conduction anisotropy—a model of spiral wave interaction with electrical remodeling of heart tissue. *Journal of Biological Physics*, 39:67–80.

Langton, C. G. (1996). Artificial life. In Boden, M. A., editor, *The Philosophy of Artificial Life*, pages 40–94. Oxford University Press.

Lim, H. S., Zipes, D. P., Hocini, M., Sacher, F., Haissaguerre, M., and Ja"is, P. (2016). Mechanisms for the termination of atrial fibrillation by localized ablation: computational and clinical studies. *Circulation: Arrhythmia and Electrophysiology*, 9(2):e003739.

Nattel, S. (2002). New ideas about atrial fibrillation 50 years on. *Nature*, 415(6868):219–226.

Pandit, S. V. and Jalife, J. (2013). Rotors and the dynamics of cardiac fibrillation. *Circulation Research*, 112(5):849–862.

Pertsov, A. M., Davidenko, J. M., Salomonsz, R., Baxter, W. T., and Jalife, J. (1993). Spiral waves of excitation underlie reentrant activity in isolated cardiac muscle. *Circulation Research*, 72:631–650.

Qu, Z., Xie, Y., Garfinkel, A., and Weiss, J. N. (2006). Critical mass hypothesis revisited: role of dynamical wave stability in spontaneous termination of cardiac fibrillation. *American Journal of Physiology—Heart and Circulatory Physiology*, 290(1):H255–H263.

Reyes, L. and Laroze, D. (2022). Cellular automata for excitable media on a complex network: The effect of network disorder in the collective dynamics. *Physica A*, 588:126552.

Romitti, G. S. et al. (2025). Implementation of a cellular automaton for efficient simulations of atrial arrhythmias. *Medical Image Analysis*, 101:103484.

Song, E. (2023). Impact of noise on the instability of spiral waves in stochastic 2d mathematical models of human atrial fibrillation. *Journal of Biological Physics*, 49:521–533.

Spector, P. S. and Bates, J. H. T. (2012). Ablation of multi-wavelet re-entry: general principles and in silico analyses. *EP Europace*, 14(suppl$_5$) : $v106 - -v111$.

Trayanova, N. A. (2014). Mathematical approaches to understanding and imaging atrial fibrillation: Significance for mechanisms and management. *Circulation Research*, 114(9):1516–1531.

Weimar, J. R., Tyson, J. J., and Watson, L. T. (1992). Diffusion and wave propagation in cellular automaton models of excitable media. *Physica D: Nonlinear Phenomena*, 55(3–4):309–327.

Winfree, A. T. (1989). Electrical instability in cardiac muscle: phase singularities and rotors. *Journal of Theoretical Biology*, 138(3):353–405.